Photoluminescence modulation in the graphene oxide dispersed 4-n-octyl-4'-cyanobiphenyl molecular system

M.S. Sannaikar, S.R. Inamdar, Benoît Duponchel, Redouane Douali, Asmita Shah, Dharmendra Pratap Singh

Photoluminescence modulation in the graphene oxide dispersed 4-n-octyl-4'-cyanobiphenyl molecular system

A. Shah,[a] M. S. Sannaikar,[b] S. R. Inamdar,[b] B. Duponchel,[c] R. Douali[a] and D. P. Singh,[*a]

[a] *Univ. Littoral Côte d'Opale, UR 4476, UDSMM, Unité de Dynamique et Structure des Matériaux Moléculaires, F-62228 Calais, France.*

[b] *Laser Spectroscopy Programme, Department of Physics, Karnatak University, Dharwad-580003, India.*

[c] *Univ. Littoral Côte d'Opale, UR 4476, UDSMM, Unité de Dynamique et Structure des Matériaux Moléculaires, F-59140 Dunkerque, France.*

Abstract

Herein, we investigate the mechanism of photoluminescence modulation (PLM) in the 4-n-octyl-4'-cyanobiphenyl liquid crystal (LC) in the presence of various doping concentrations (0.02 to 0.4 wt%) of 2D-GO (two-dimensional graphene oxide) nanoflakes. The role of intermolecular interactions on PLM and the subsequent effect on the decay lifetime is also examined via time-resolved PL measurements. The presence of intermolecular interactions is additionally confirmed by means of differential scanning calorimetry and polarized optical microscopy. The successive addition of GO nanoflakes sharpens the absorption band of pure 8CB LC; consequently, it is blue shifted. The PL properties of the 8CB LC enhance due to the addition of GO nanoflakes which might be attributed to electron-phonon interaction between 8CB molecules and GO nanoflakes. The PL enhancement has been further supported by the time-resolved PL decay time measurement. The longest and shortest fluorescence lifetimes have been recorded for the 0.1 and 0.4 wt % GO/8CB composites, respectively. The investigated composites have shown their potential applications for fluorescent optical devices; however, the quantum efficiency needs to be further improved.

Keywords: Liquid crystal material; Graphene oxide; Photoluminescence; UV-visible absorbance; fluorescence decay lifetime.

1. Introduction

After the first demonstration of polarised organic light-emitting diodes (OLEDs) in 1995, luminescent liquid crystalline (LLC) materials have attracted immense interests for organic optoelectronic applications, in particular the linearly polarised emission, as it combines the easy alignment of molecules and their luminescence properties [1, 2]. Calamitic LC materials are comparatively insignif-

Preprint submitted to Journal of Luminescence *June 21, 2020*

[*]Corresponding author, Tel.:+33 (0)321465758, Email: Dharmendra.Singh@univ-littoral.fr

icant for OLED application in comparison to the discotic LC materials which shows visible light emission [3, 4]. In contrast, calamitic LC exhibits the ultraviolet absorption and emission that could also be transformed via doping a nanostructured materials [5, 6, 7, 8, 9, 10, 11, 12, 13]. Such transformation in PL property of a host matrix remarkably depends on several factors like shape, size, concentration, excitation wavelength, etc. of the guest dopant. Moreover, the absorption and emission properties of the dopant is one of the factors that determines the overall PL properties of the composites. For example, the behavior of metallic [13], semiconducting [7] and insulating nanoparticles [9, 11] in the liquid crystalline matrices is found to be completely state of affairs for enhancing or quenching the PL properties. Some reports show the enhancement in PL emission of the LC materials due to the dispersion of different nanoparticles [9, 13]; meanwhile, on the other hand, the presence of quantum materials has quenched photoluminescence of LCs [14, 15, 16]. Moreover, the incorporation of specific nanoparticles has also produced an induced photoluminescence in a non-luminescent LC material [17]. Despite using several kinds of nanoparticles and quantum dots, fewer investigations have been carried out with the two-dimensional (2D) nanosheets or flakes like graphene oxide (GO) or reduced graphene oxide (rGO) [18, 19].

Graphene shows superior electronic and mechanical properties as compared to its mother element graphite and it represents a single layer of graphite, in which sp^2 bonded carbon atoms are hexagonally arranged. GO is derived from graphite by chemical oxidation and subsequent exfoliation and it is readily dispersible in aqueous medium. The physical properties of GO depend on the degree of oxidation. The dispersion of graphene, GO and rGO has revealed some superior properties in the LCs [20, 21, 22, 23, 24]. The most of investigated regimes with the dispersion of graphene, GO and rGO include the study of electro-optical, electronic and thermal properties, but it has not been done so well for the photoluminescence. Therefore, this field has plenty of opportunities for further investigations to realize better composites for next-generation fluorescent displays and photonic devices.

In our previous article [23], we have investigated the graphene oxide (GO) dispersed 4-n-octyl-4'-cyanobiphenyl (8CB) hybrid system to disclose the long-range molecular interactions between GO and 8CB molecules. In this report, it has been seen that the orientation of 8CB molecules successively changes from planar to homeotropic depending on the dispersion concentration of GO. This study was focused on the molecular interaction and electronic properties of the hybrid system, but the investigation of photophysical properties for the hybrid system along with the pristine 8CB material has not been performed so far; therefore, in the present article, we have quantitatively studied the photoluminescence modulation in the 4-n-octyl-4'-cyanobiphenyl (8CB) liquid crystalline material dispersed with various concentrations of 2D-graphene oxide nanoflakes. The photoluminescence modulation (PLM) depends upon the intermolecular interactions between the 8CB molecules and the 2D-GO nanoflakes. The reduction in full width at half maxima (FWHM) of the absorption band and slight shifting in the PL band supports the existence of intermolecular interactions.

The underlined mechanism has been further supported by the time-resolved PL measurements. The investigated composites indicate their applications for optical energy storage which is discussed within the scope of this paper.

2. Experimental details

2.1. Host material: 4-n-octyl-4'-cyanobiphenyl (8CB) liquid crystal material

Figure 1(a) represents the molecular structure of the 4-n-octyl-4'-cyanobiphenyl (8CB) liquid crystalline material. It exhibits smectic A and nematic mesophases including the transitions between crystalline and smectic A phases. The phase sequence of the 8CB LC material is as follows-

Smectic A 33.63 (0.32) Nematic 40.72 (3.68) Isotropic [in heating cycle]
Isotropic 40.57 (4.44) Nematic 33.33 (0.50) Smectic A [in cooling cycle]

Transition temperatures are represented in ^{o}C and corresponding transition enthalpies, shown in the brackets, are mentioned in $\mathrm{J\,g^{-1}}$. The FTIR and NMR data fo the 8CB LC material is given as supplementary information.

2.2. Dopant material: Graphene oxide nanoflakes

2D-GO nanoflakes were synthesized from commercially available graphite following the Hummers method as previously described in our previous articles [18, 19, 23]. We have utilized the same 2D-GO nanoflakes in this study which is already reported in our previous articles [19, 23]. To prepare GO suspension in DMF, 0.65 mg of 2D-GO nanoflakes were dissolved in 160 microliter of DMF and sonicated for 2.5 hours. This suspension was deposited on a Si wafer by drop casting technique and dried for 4 hours at 50 ^{o}C. The SEM image of 2D-GO nanoflakes is presented in figure 1(b). The width size distribution of 2D-GO nanoflakes was in the range of 10–40 nm, whereas the lateral size distribution was found to be $\approx$ 50 nm–25 μm. As the characterization data of 2D-GO nanoflakes have already been published; therefore, we are not providing all characterization data here and only referring to the size and SEM image of nanoflakes.

2.3. Preparation of the 8CB/GO composites

0.1 $\mathrm{mg\,ml^{-1}}$ suspension of 2D-GO was first prepared in the toluene. The suspension was homogenized by ultrasonication for several hours. After obtaining a homogenous suspension, it was added to the 8CB LC maintaining the wt/wt% from 0.02 to 0.4. The higher dispersion concentrations of GO were deferred as they started showing a high tendency of agglomeration beyond the 0.4 wt%.

2.4. Differential scanning calorimetry (DSC)

Usually, the dispersion of an external guest dopant causes the shifting of the mesophase transition temperatures of a LC material; therefore, it is essential to study the phase transitions of the 8CB/GO composites. For this purpose, phase thermograms were obtained using the TA Instruments Q1000 differential scanning calorimeter with a 2 $\mathrm{K\,min^{-1}}$ heating/cooling rate. Later on, the DSC thermograms were normalized according to the weight of the samples taken for the DSC study.

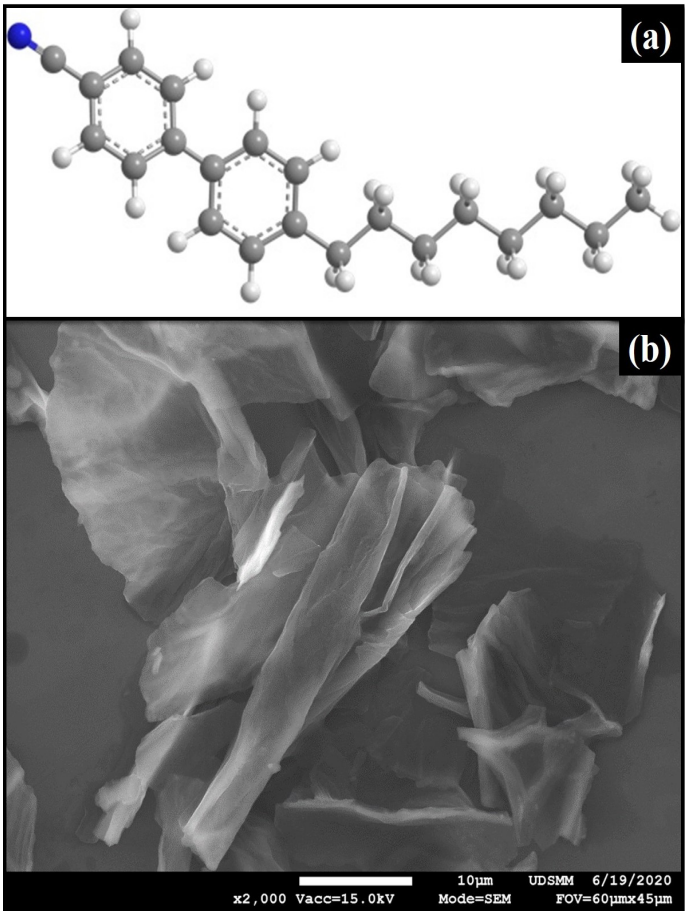

Figure 1: (a) Molecular structure of the 4-n-octyl-4'-cyanobiphenyl (8CB) liquid crystalline material and (b) scanning electron microscopic (SEM) image of 2D-graphene oxide (2D-GO) nanoflakes.

2.5. Polarized optical microscopy (POM)

Polarized optical microscopy is a fundamental tool to ensure the homogenous distribution of dopants in a LC matrix; therefore, polarized optical microscopic (POM) observations were performed on the ZEISS AXIO equipped with Infinity2 image capturing software. During the POM measurements, the temperature of materials was controlled with a Linkam TMS 94 hotstage. The pure 8CB and its GO nanoflakes composites were filled in 50 μm thick unaligned commercial sample cells (purchased from AWAT, Poland) to perform polarized optical microscopy.

2.6. UV-visible absorption spectroscopy

UV-visible absorption measurements were performed using a NIR-UV-VIS Spectrophotometer (Jasco, V670). UV-visible spectra were recorded in the solution state (concentration = 1 $\mathrm{mg\,ml^{-1}}$), using toluene as solvent [11, 12]. Absorption measurements were carried out in the range from 200 to 750 nm by keeping the both entrance and exit slit width equal to 5nm. The baseline and background corrections were done before performing the absorption measurements for the pristine 8CB LC and mixtures.

2.7. Photoluminescence (PL) studies

The photoluminescence spectra of pure 8CB and its 2D-GO composites were recorded with the help of a Fluoromax-4 Spectrofluorometer (JY, Horiba). All the samples were excited by a monochromatic light of wavelength 300 nm since the 8CB and 8CB/GO composites have a strong absorption band at this wavelength as rendered from UV-visible absorption measurements.

2.8. Time-resolved PL Measurements (TRPL)

In steady-state spectral measurement, the detector adds up all the photons emitted by the sample molecules, starting with the instance of excitation and ending with a time when the last excited molecule is decayed to the ground state. Time-resolved measurements, using time correlated single photon counting (TCSPC) technique, were performed; since they contain more information than is available from the steady-state data. Owing to spectral overlap of absorption and emission, it is usually not possible to resolve the emission from the multiple residues from the steady-state data. Further, one can distinguish between static and dynamic quenching using lifetime measurements. Moreover, probe concentration can change during the measurement due to photobleaching leading to difficulty in making quantitative use of the local intensities. In contrast, fluorescence lifetimes are typically independent of the probe concentration and are not influenced by the fluctuations in the lamp intensity. We have used a pulsed LED as an excitation source (296 nm) to measure the decay times of these composites at their maximum PL peak using a time-domain based ISS ChronosBH TCSPC Spectrometer. All the optical measurements were carried out at room temperature.

3. Results and discussion

3.1. Differential scanning calorimetric (DSC) study

The effect of GO dispersion on the mesophase transition temperatures of the 8CB LC material has been studied. Figure 2 shows the normalized differential scanning calorimetric (DSC) curves of the 8CB and its composites having different concentrations of 2D-GO nanoflakes. As stated in the experimental section, the 8 CB LC exhibits smectic A (SmA) and nematic (N) mesophases. The SmA-N and N-Iso phase transitions took place at 33.63 and 40.72 ^{o}C, respectively during the heating process. It is observed in all composites that

the addition of different concentrations of GO in the 8CB causes a lowering in the N-Iso phase transition temperature. As the nematic-to-isotropic (N−I) is a weakly first-order transition; therefore, it might be due to lowering of the orientational order of the pure 8CB material after the dispersion of GO into different concentrations. In addition to this, it is also observed that the SmA-N phase transition has been weakened. It is probably due to lowering in the positional order of the SmA phase originated because of the change in layer arrangement. Usually, 2D-GO nanoflakes align with orientational directions along their long axes and the 8CB molecules tend to align along with the flakes; however, the global orientation does not relay in a single direction resulting in the reduction in the order parameter.

3.2. Polarized optical microscopic study

Polarized optical micrographs (POMs) of the 8CB and its GO nanoflakes composites are presented in figure 3. In general, the molecules of the pure 8CB LC material preferentially orient along with the director ($\vec{n}$). The pristine 8CB LC material renders the typical fan-shaped texture of in smectic A phase (figure 3a, at 25 ^{o}C) and traditional schlieren texture in the nematic phase (figure 3b, at 35 ^{o}C). The temperature for recording the POMs of 8CB/GO composites in a desired phase was chosen from their corresponding phase schemes. It is observed that the presence of 2D-GO flakes significantly changes the molecular orientation of the 8CB; as a result, the exemplary optical textures of the SmA and N phases have not been observed for the composites because of the GO flakes migrate closer to ITO substrate/LC interface due to viscous drift [23]. As the dispersion concentration of GO is successively increased, the molecular orientation of the 8CB changes accordingly, and a homeotropic orientation has been achieved for the dispersion 0.4 wt% of GO. At this particular concentration of GO, global homeotropic orientation is visible (figure 3k,l); however, some illuminated regions are also observed which is might be due to the scattering of incident light through the edges of GO flakes. The observed homeotropic orientation is because of the interaction between the polar C≡N functional group of the 8CB molecules with the GO surface via an electron-phonon interaction. This postulate is recently reported by us [23]. For the intermediate dispersion concentration of 2D-GO nanoflakes, the orientation of 8CB molecules represents a merged state of the planar and homeotropic orientations.

3.3. UV-visible absorption study

The absorption spectrum of any material is the result of its electronic, vibrational, and rotational transitions. The absorption peak corresponds to the electronic transition line, and the rest of the spectrum is formed by a series of lines that correspond to rotational and vibrational transitions. Therefore, the absorption spectrum provides in-depth information about the structure and transitions. The UV-visible absorption spectra of the pure 8CB LC and 8CB/2D-GO nanoflakes composites containing different GO concentrations (i.e. 0.02, 0.1, 0.2, 0.3 and 0.4 wt%) were recorded. These spectra were taken in the

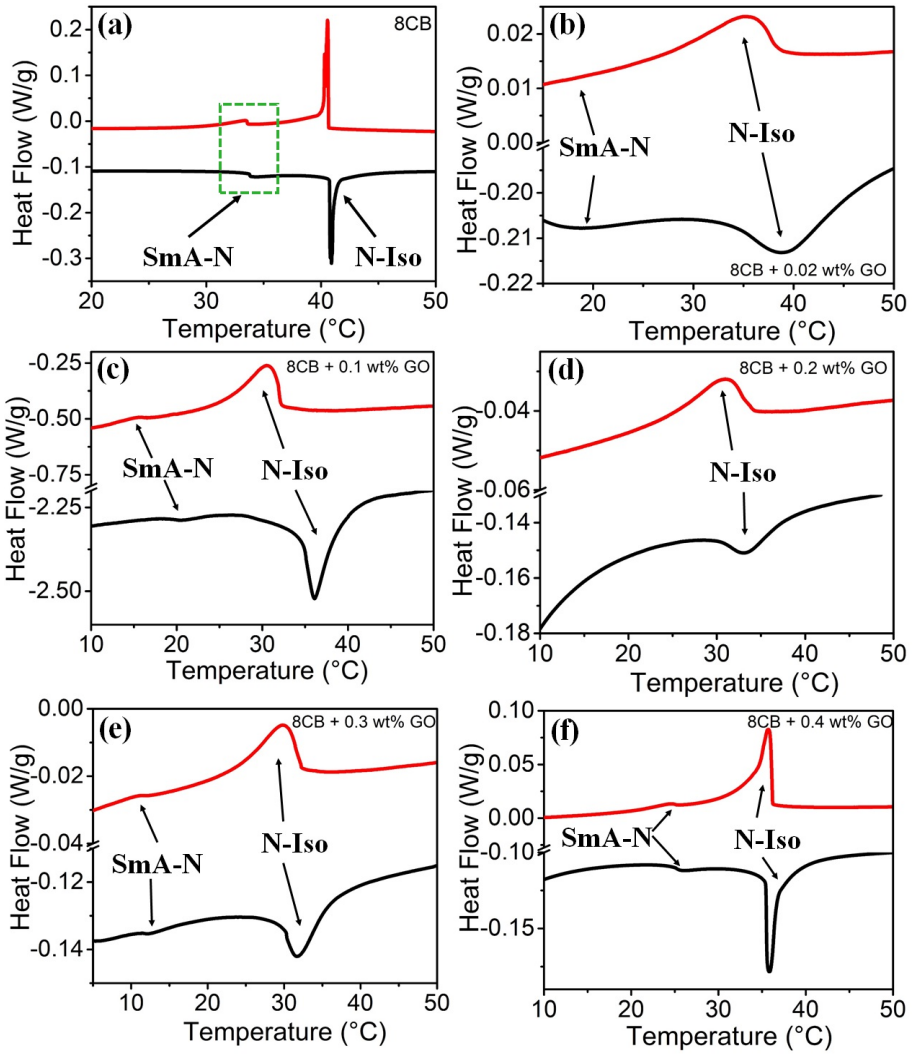

Figure 2: Normalized differential scanning calorimetric (DSC) curves of (a) 8CB, (b) 8CB + 0.02, (c) 8CB + 0.1, (d) 8CB + 0.2, (e) 8CB + 0.3 and (d) 8CB + 0.4 wt% dispersion of 2D-GO nanoflakes with a heating/cooling rate of 2 K min^{-1}.

solution having toluene as solvent and 1mg/ml solution concentration. Figure 4 shows the normalized absorption spectra of the pure 8CB LC and 8CB/2D-GO nanoflakes composites.

It is noticed that the 8CB LC shows a strong absorption band nearly at 300 nm which is attributed to π-π^* transitions in $^1A_{1g}-^1B_{1u}$. The $^1A_{1g}-^1B_{1u}$ is a spin allowed, symmetry-forbidden, but vibronically allowed transition [25]. Additionally, we have previously reported that the 2D-GO flakes exhibit two ab-

sorption peaks at 230 and 300 nm,(supplementary figure S1), attributed to π–π^* transitions of C=C bonds and to n–π^* transitions of C=O bonds, respectively [19, 26]. In 8CB/2D-GO composites, the successive addition of increasing weight concentration of GO results a trivial narrowing in the absorption bandwidth. Inset of figure 4 depicts the full-width half maxima (FWHM) for the pure 8CB and 8CB/2D-GO nanoflakes composites. The FWHM varies nonlinearly with the increasing concentration of GO nanoflakes in the solution. Besides, the narrowing in the FWHM of the absorption band also caused a feeble blue shifting. Steady-state spectral parameters are represented in Table 1. The sharpening in the UV-visible absorption spectra of the 8CB/GO composites can be explained by the modified Beer-Lambert law [27], which is as follows-

$$I = I_o(-c)^n exp(\epsilon l) \tag{1}$$

where, I_o and I are the intensities of the incident and transmitted radiations, respectively. c and l are the solution concentration and optical path length, respectively, and ϵ is the absorption coefficient. n is the power exponent.

In our study, the sharpness of the absorption band (slightly blue shifting) might be associated with the dipole-dipole interactions between the 8CB LC molecules and GO nanoflakes. If the dipole-dipole interaction is strong, the energy required for an absorption will also be large, i.e., the position of the absorption band will be located at lower wavelengths [28, 29].

3.4. Photoluminescence (PL) study

The room temperature PL spectra of the pure 8CB LC and its composites with GO nanoflakes are presented in figure 5. The pure 8CB LC exhibits a strong PL emission peak at 336 nm, whereas 2D-GO nanoflakes emit a violet band of 362 nm, (see supplementary figure S2), attributed to the n–π^* transition of the isolated sp^2 domains within the carbon-oxygen sp^3 matrix [19, 26]. In this study, we have not contemplated about the contribution of the disorder-induced long-wavelength PL band (visible at $\approx$ 700 nm) of the GO nanoflakes as the 8CB/GO composites only show a single PL emission nearly at 340 nm. Interestingly, PL intensity of the 8CB/GO composites increases as compared to the pure 8CB LC. This modulation in the PL emission might be related to the combined effect of the change in optical density of 8CB LC after the addition of different concentrations of GO nanoflakes and electron-phonon interaction between the 8CB molecules and GO surface. In addition to this, the change in molecular orientation could also be a factor that leads to PL modulation in the composites. The optical density of a material is related to the PL emission in the following manner.

At a particular excitation wavelength, the PL emission intensity can be explained as follows [29]-

$$I_{PL(\lambda)} = 2.3 I_O \epsilon_{(\lambda)} cl \phi_{PL} \tag{2}$$

where,ϕ_{PL} is the photoluminescence quantum yield and other abbreviations are the same as explained in equation 1.

It is clear by the aforementioned equation that the PL intensity is proportional to the optical density i.e. ϵcl. With the addition of GO nanoflakes in the 8CB LC, optical density changes nonlinearly due to the interfacial properties of GO surface and 8CB molecules that govern the changes in the PL emission.

Besides, a nonlinearity in the PL emission as a function of GO concentration for the 8CB/GO composites has also been observed. For the composites, maximum and minimum PL intensities have been observed for the 0.4 and 0.3 wt% of GO, respectively. In addition to the change in the PL intensity, the broadening of the PL band has also changed. The change in the broadening of the PL band is probably due to the contribution of the PL of GO nanoflakes. We have also analyzed this nonlinear change in the photophysical property by plotting the Stokes shift versus GO concentration in the 8CB LC which is shown in figure 6. A maximum Stokes shift (difference between the emission and absorption peak wavelengths) of about 48 nm is detected for 0.1 % wt GO. A comparison of the steady-state spectral properties of the 8CB LC and its composites with various GO nanoflakes concentrations are listed in Table 1.

The fluorescence quantum yield of a sample is determined using a relative optical method. The absorption factor should be estimated accurately for solutions with a low absorbance, typically A $\cong$ 0.1, to avoid internal filter effects and errors arising from uneven distribution of the excited species in the detected volume. The fluorescence quantum yields (φ_s) were obtained by comparison with a standard dye using Equation-

$$\varphi_s = \varphi_r \left(\frac{I_s A_r n_s^2}{I_r A_s n_r^2} \right) \tag{3}$$

where, I_s and I_r are the integrated fluorescence emissions of the samples (binary mixtures) and the standard dye (Coumarin 440, QY = 0.98) in ethanol, respectively [30]. A_s and A_r, respectively, are the absorbances at the excitation wavelength of the samples and the reference, while φ_s and φ_r, respectively, are the quantum yields of the sample and the reference, n being the refractive index. The values of I_s and I_r are determined from the photoluminescence spectra corrected for the instrumental response, by integrating the emission intensity over the desired spectral range.

The results substantiate that the monotonical increase of quantum yield for 0.02, 0.2 and 0.4wt% of GO is in accordance with the results of photoluminescence modulation of 8CB upon addition of GO. Further, quantum efficiency for 0.1 and 0.2 wt% of GO are more as compared to that of pure 8CB. Hence, GO has modulated and enhanced the photoluminescence properties of the 8CB system.

3.5. Time Resolved Photoluminescence Measurements (TRPL)

The fluorescence decay profiles of the pure 8CB LC and 8CB/GO composites are presented in figure 7. The decay curves were fitted by a bi-exponential decay function and results are listed in Table 2. The average decay lifetime, ($\langle\tau\rangle$), was calculated from the following equation [27]-

$$\langle \tau \rangle = \frac{\tau_1 A_1 + \tau_2 A_2}{A_1 + A_2} \quad (4)$$

where, τ_1 and τ_2 represents the shorter and longer lifetime components with their normalized amplitude components A_1 and A_2, respectively. The fast decay process with a lifetime around 1 ns,(τ_1), can be attributed to the non-radiative re-combination, while the slow decay process (τ_2) originates from the radiative decay.

The pure 8CB LC has a fluorescence decay lifetime of 1.32 ns; however, after the dispersion of GO into various proportions, the decay lifetime also changes. The gradually increasing dispersion concentration of GO in the 8CB LC from 0.0 to 0.1 wt % leads to an enhancement of the decay lifetime from 1.32 ns to 1.81 ns. Further addition of GO into the 8CB LC, reduces the decay lifetimes. The longest fluorescence lifetime is detected for the 8CB+0.1 wt % GO composite; whereas, the shortest decay lifetime is noticed for the 0.4 wt % GO/8CB composite. The variation of average decay lifetime of the 8CB LC and its composites with different concentrations of 2D-GO nanoflakes is presented in figure 8. The increased decay lifetimes indicate that the PL properties of the 8CB LC have been enhanced after the dispersion of GO concentration up to 0.1 wt%. In this situation, PL decays are dominated by the radiative process. Beyond this critical concentration, average decay lifetime decreases which suggests that the non-radiative decay processes are taking place in the composites and might be resulting in the quenching of PL intensity. This study indicates that the small dispersion concentration of 2D-GO nanoflakes are superior in PL properties; thus, such composites could be used for fluorescent displays and optical devices.

4. Conclusions

In conclusion, various concentrations of 2D-GO nanoflakes were dispersed in a commercially available 4-n-octyl-4'-cyanobiphenyl (8CB) liquid crystalline (LC) material and characterized via differential scanning calorimetry (DSC), polarized optical microscopy, UV-visible, photoluminescence and time-resolved PL techniques. DSC thermograms reveal that the dispersion of GO nanoflakes lowers the weakly first-order nematic-isotropic (N-Iso) phase transition temperature. This lowering of the N-Iso phase transition temperature might be due to weaker orientational order parameter in the composites. The change in the smectic A to nematic (SmA-N) phase transition is associated with the reduction of positional ordering in the composites. 8CB LC exhibits a strong absorption band at 300 nm attributing to the π-π^* transitions, whereas GO nanoflakes show two absorption peaks at 230 and 300 nm attributed to π–π^* transitions of C=C bonds and to n–π^* transitions of C=O bonds, respectively. The dispersion of GO nanoflakes causes the sharpening of the absorption band which has been explained by the modified Beer-Lambert law. The presence of GO nanoflakes has enhanced the PL emission of 8CB LC which is probably associated with the combined effects of electron-phonon interaction and change in optical density.

The enhancement in PL properties has been further supported by the time-resolved PL measurements. The longest fluorescence lifetime has been detected for the 8CB+0.1 wt % GO composite; whereas, the shortest decay lifetime is noticed for the 0.4 wt % GO/8CB composite and their recorded values were found to be 1.81 and 1.06 ns, respectively. All the optical properties including the quantum efficiency were found to be nonlinear as a function of GO concentration. The nonlinearity in the optical properties might be due to the interfacial properties of 8CB molecules and GO surface. The enhanced PL properties for small dispersion concentration of GO nanoflakes would be interesting for the fluorescent displays and optical devices.

Acknowledgment

DPS gratefully acknowledges the financial assistance provided by the UDSMM, ULCO. Prof. A. Hadj Sahraoui, Director UDSMM is highly acknowledged for his kind support. We are thankful to Prof. François Delattre and Mr. Steven Ruellan for his help in NMR measurement.

Conflict of interest

The article is original and has been written by the stated authors who are aware of its content and approve its submission. This article has neither been published previously nor under consideration for the publication elsewhere. We also declare "No conflict of interest exists".

References

[1] Y. Wang, J. Shi, J. Chen, W. Zhu, E. Baranoff, Recent progress in luminescent liquid crystal materials: design, properties and application for linearly polarised emission, Journal of Materials Chemistry C 3 (31) (2015) 7993–8005. doi:10.1039/C5TC01565K.
URL https://pubs.rsc.org/en/content/articlelanding/2015/tc/c5tc01565k

[2] L. He, J. Ye, M. Shuai, Z. Zhu, X. Zhou, Y. Wang, Y. Li, Z. Su, H. Zhang, Y. Chen, Z. Liu, Z. Cheng, J. Bao, Graphene oxide liquid crystals for reflective displays without polarizing optics, Nanoscale 7 (5) (2015) 1616–1622. doi:10.1039/C4NR06008C.
URL http://pubs.rsc.org/en/content/articlelanding/2015/nr/c4nr06008c

[3] A. Gowda, L. Jacob, D. P. Singh, R. Douali, S. Kumar, Charge Transport in Novel Phenazine Fused Triphenylene Supramolecular Systems, ChemistrySelect 3 (23) (2018) 6551–6560. doi:10.1002/slct.201801412.
URL https://onlinelibrary.wiley.com/doi/abs/10.1002/slct.201801412

[4] I. Bala, W.-Y. Yang, S. P. Gupta, J. De, R. A. K. Yadav, D. P. Singh, D. K. Dubey, J.-H. Jou, R. Douali, S. K. Pal, Room temperature discotic liquid crystalline triphenylene-pentaalkynylbenzene dyads as an emitter in blue OLEDs and their charge transfer complexes with ambipolar charge transport behaviour, Journal of Materials Chemistry C 7 (19) (2019) 5724–5738. doi:10.1039/C9TC01178A.
URL https://pubs.rsc.org/en/content/articlelanding/2019/tc/c9tc01178a

[5] D. P. Singh, S. Kumar Gupta, S. Pandey, K. Singh, R. Manohar, Electro-optical, UV absorbance, and UV photoluminescence analysis of Se95In5 chalcogenide glass microparticle doped ferroelectric liquid crystal, Journal of Applied Physics 115 (21) (2014) 214103. doi:10.1063/1.4880997.
URL https://aip.scitation.org/doi/full/10.1063/1.4880997

[6] P. Goel, M. Arora, A. M. Biradar, Evolution of excitation wavelength dependent photoluminescence in nano-CeO2 dispersed ferroelectric liquid crystals, RSC Advances 4 (22) (2014) 11351–11356. doi:10.1039/C3RA47225F.
URL http://pubs.rsc.org/en/content/articlelanding/2014/ra/c3ra47225f

[7] T. Joshi, P. Ganguly, D. Haranath, S. Singh, A. M. Biradar, Tuning the photoluminescence of ferroelectric liquid crystal by controlling the size of dopant ZnO quantum dots, Materials Letters 114 (2014) 156–158. doi:10.1016/j.matlet.2013.09.110.
URL http://www.sciencedirect.com/science/article/pii/S0167577X13013542

[8] M. Kumar, S. Kumar, Stacking of ultra-thin reduced graphene oxide nanoparticles in supramolecular structures for optoelectronic applications, RSC Advances 5 (19) (2015) 14871–14878. doi:10.1039/C4RA15705B.
URL http://pubs.rsc.org/en/content/articlelanding/2015/ra/c4ra15705b

[9] J. S. Roy, T. Pal Majumder, R. Dabrowski, Photoluminescence behavior of TiO2 nanoparticles doped with liquid crystals, Journal of Molecular Structure 1098 (2015) 351–354. doi:10.1016/j.molstruc.2015.06.028.
URL http://www.sciencedirect.com/science/article/pii/S0022286015300533

[10] D. P. Singh, T. Vimal, Y. J. Mange, M. C. Varia, T. Nann, K. K. Pandey, R. Manohar, R. Douali, CuInS2/ZnS QD-ferroelectric liquid crystal mixtures for faster electro-optical devices and their energy storage aspects, Journal of Applied Physics 123 (3) (2018) 034101. doi:10.1063/1.5021474.
URL https://aip.scitation.org/doi/10.1063/1.5021474

[11] D. P. Singh, K. Agrahari, A. S. Achalkumar, C. V. Yelamaggad, R. Manohar, M. Depriester, Preparation and photophysical properties of soft-nano composites comprising guest anatase TiO2 nanoparticle and host hekates mesogens, Journal of Luminescence 205 (2019) 304–309. doi:10.1016/j.jlumin.2018.09.035.
URL http://www.sciencedirect.com/science/article/pii/S0022231318310755

[12] D. P. Singh, A. K. Misra, A. S. Achalkumar, C. V. Yelamaggad, M. Depriester, Transmuting the blue fluorescence of hekates mesogens derived from tris(N-salicylideneaniline)s core via ZnS/ZnS:Mn2+ semiconductor quantum dots dispersion, Journal of Luminescence 210 (2019) 7–13. doi:10.1016/j.jlumin.2019.02.009.
URL http://www.sciencedirect.com/science/article/pii/S0022231318319136

[13] A. Roy, K. Agrahari, A. Srivastava, R. Manohar, Plasmonic resonance instigated enhanced photoluminescence in quantum dot dispersed nematic liquid crystal, Liquid Crystals 46 (8) (2019) 1224–1230. doi:10.1080/02678292.2018.1549283.
URL https://doi.org/10.1080/02678292.2018.1549283

[14] D. P. Singh, S. Pandey, S. Gupta, R. Manohar, A. Daoudi, A. Sahraoui, C. Phadnis, S. Mahamuni, Quenching of photoluminescence and enhanced contrast of ferroelectric liquid crystal dispersed with Cd 1-X Zn X S/ZnS core/shell nanocrystals, Journal of Luminescence 173 (2016) 250–256. doi:10.1016/j.jlumin.2015.12.042.
URL http://linkinghub.elsevier.com/retrieve/pii/S0022231315301393

[15] D. P. Singh, A. Daoudi, S. K. Gupta, S. Pandey, T. Vimal, R. Manohar, A. K. Kole, P. Kumbhakar, A. Kumar, Mn2+ doped ZnS quantum dots in ferroelectric liquid crystal matrix: Analysis of new relaxation phenomenon, faster optical response, and concentration dependent quenching in photoluminescence, Journal of Applied Physics 119 (9) (2016) 094101. doi:10.1063/1.4942663.
URL https://aip.scitation.org/doi/abs/10.1063/1.4942663

[16] D. P. Singh, B. Duponchel, K. Kondratenko, Y. Boussoualem, G. H. Pujar, S. Inamdar, R. Douali, A. Daoudi, Phase Contraction, fluorescence quenching and formation of topological defects in chiral smectic C matrix by $Cd_{0.15}Zn_{0.85}S$/ZnS core/shell quantum dots dispersion: Faster electro-optic response for gadget displays, Liquid Crystals (2020). doi:10.1080/02678292.2020.1754939.

[17] D. P. Singh, S. K. Gupta, A. Srivastava, R. Manohar, The phenomenon of induced photoluminescence in ferroelectric mesophase, Journal of Luminescence 139 (2013) 60–63. doi:10.1016/j.jlumin.2013.02.037.
URL http://linkinghub.elsevier.com/retrieve/pii/S0022231313000938

[18] D. P. Singh, V. Kumar, A. Kumar, R. Manohar, R. Pasricha, B. Duponchel, Y. Boussoualem, A. H. Sahraoui, A. Daoudi, Effect of graphene oxide interlayer electron-phonon coupling on the electro-optical parameters of a ferroelectric liquid crystal, RSC Advances 7 (21) (2017) 12479–12485. doi:10.1039/C6RA25126A.
URL http://xlink.rsc.org/?DOI=C6RA25126A

[19] D. P. Singh, B. Duponchel, Y. Boussoualem, K. Agrahari, R. Manohar, V. Kumar, R. Pasricha, G. H. Pujar, S. R. Inamdar, R. Douali, A. Daoudi,

Dual Photoluminescence and Charge Transport in alkoxy biphenyl benzoate ferroelectric liquid crystalline-Graphene Oxide Composite, New Journal of Chemistry 42 (2018) 16682–16693. doi:10.1039/C8NJ02985G.
URL https://pubs.rsc.org/en/content/articlelanding/2018/nj/c8nj02985g

[20] R. T. M. Ahmad, S.-H. Hong, T.-Z. Shen, J.-K. Song, Optimization of particle size for high birefringence and fast switching time in electro-optical switching of graphene oxide dispersions, Optics Express 23 (4) (2015) 4435–4440. doi:10.1364/OE.23.004435.
URL https://www.osapublishing.org/oe/abstract.cfm?uri=oe-23-4-4435

[21] R. Basu, D. Kinnamon, N. Skaggs, J. Womack, Faster in-plane switching and reduced rotational viscosity characteristics in a graphene-nematic suspension, Journal of Applied Physics 119 (18) (2016) 185107, publisher: American Institute of Physics. doi:10.1063/1.4949481.
URL https://aip.scitation.org/doi/10.1063/1.4949481

[22] S. Özgan, H. Eskalen, Y. Tapkıranlı, Thermal and electro-optic properties of graphene oxide-doped hexylcyanobiphenyl liquid crystal, Journal of Theoretical and Applied Physics 12 (3) (2018) 169–176. doi:10.1007/s40094-018-0307-y.
URL https://doi.org/10.1007/s40094-018-0307-y

[23] D. P. Singh, B. Duponchel, Y. Lin, J.-F. Blach, H. Khemakhem, C. Legrand, R. Douali, Orientation of 4-n-octyl-4–cyanobiphenyl molecules on graphene oxide surface via electron-phonon interaction and its applications in nonlinear electronics, J. Mater. Chem. C 7 (9) (2019) 2734–2743. doi:10.1039/C8TC05696J.
URL http://dx.doi.org/10.1039/C8TC05696J

[24] D. P. Singh, A. K. Misra, K. K. Pandey, B. Pal, N. Kumar, D. Singh, K. Kondratenko, B. Duponchel, P. Genevray, R. Douali, Spectroscopic, dielectric and nonlinear current–voltage characterization of a hydrogen-bonded liquid crystalline compound influenced via graphitic nanoflakes: An equilibrium between the experimental and theoretical studies, Journal of Molecular Liquids 302 (2020) 112537. doi:10.1016/j.molliq.2020.112537.
URL http://www.sciencedirect.com/science/article/pii/S016773221936773X

[25] D. Singh, S. Pandey, R. Manohar, S. Kumar, G. Pujar, S. Inamdar, Time-resolved fluorescence and absence of Förster resonance energy transfer in ferroelectric liquid crystal-quantum dots composites, Journal of Luminescence 190 (2017) 161–170. doi:10.1016/j.jlumin.2016.09.056.
URL http://linkinghub.elsevier.com/retrieve/pii/S0022231316300369

[26] G. Eda, Y.-Y. Lin, C. Mattevi, H. Yamaguchi, H.-A. Chen, I.-S. Chen, C.-W. Chen, M. Chhowalla, Blue Photoluminescence from Chemically Derived Graphene Oxide, Advanced Materials 22 (4) (2010) 505–509. doi:10.1002/adma.200901996.
URL http://onlinelibrary.wiley.com/doi/10.1002/adma.200901996/abstract

[27] J. R. Lakowicz, Principles of Fluorescence Spectroscopy, 3rd Edition, Springer US, 2006.
URL //www.springer.com/gp/book/9780387312781

[28] P. Mahesh, A. Shah, K. Swamynathan, D. P. Singh, R. Douali, S. Kumar, Carbon dots dispersed hexabutyloxytriphenylene discotic mesogens: Structural, morphological and charge transport behavior, Journal of Materials Chemistry CPublisher: The Royal Society of Chemistry (Jun. 2020). doi:10.1039/D0TC02028A.
URL https://pubs.rsc.org/en/content/articlelanding/2020/tc/d0tc02028a

[29] J. R. Albani, Fluorescence Spectroscopy Principles, in: Principles and Applications of Fluorescence Spectroscopy, John Wiley & Sons, Ltd, 2008, pp. 88–114, section: 7 _eprint: https://onlinelibrary.wiley.com/doi/pdf/10.1002/9780470692059.ch7.
doi:10.1002/9780470692059.ch7.
URL https://onlinelibrary.wiley.com/doi/abs/10.1002/9780470692059.ch7

[30] C. Wang, L.-O. Pålsson, A. S. Batsanov, M. R. Bryce, Molecular Wires Comprising π-Extended Ethynyl- and Butadiynyl-2,5-Diphenyl-1,3,4-Oxadiazole Derivatives:FIXME Synthesis, Redox, Structural, and Optoelectronic Properties, Journal of the American Chemical Society 128 (11) (2006) 3789–3799, publisher: American Chemical Society.
doi:10.1021/ja0577600.
URL https://doi.org/10.1021/ja0577600

Tables

Sample	λ_{abs} (nm)	**FWHM**$_{abs}$ (nm)	λ_{em} (nm)	**Stokes shift** ($\Delta\lambda$, nm)	**PL Intensity** (arb. units)	**QY**
8CB	300	34.00	336	36	11838	0.0976
2D-GO nanoflakes	300	-	362	62	11335	-
8CB + 0.02 wt% GO	299	29.85	341	42	30698	0.5448
8CB + 0.1 wt% GO	297	30.10	345	48	26764	0.3951
8CB + 0.2 wt% GO	297	25.74	337	40	43419	0.6362
8CB + 0.3 wt% GO	297	30.09	337	40	19265	0.3924
8CB + 0.4 wt% GO	297	25.73	335	38	112279	0.8180
C440 (C120)			430			0.9800*

Table 1: Steady-state spectral properties of the 8CB LC and its composites having different concentrations of 2D-GO nanoflakes. QY is abbreviated for quantum yield. *Quantum yield of reference dye.

Sample	τ_1 (ns)	τ_2 (ns)	A_1 (%)	A_2 (%)	τ (ns)	χ^2
8CB	0.21	1.35	2.47	97.53	1.32	1.2209
2D-GO nanoflakes	1.29	1.15	96.81	3.19	1.28	1.2
8CB + 0.02 wt% GO	1.20	3.35	87.35	12.65	1.47	1.2506
8CB + 0.1 wt% GO	1.28	3.55	76.63	23.37	1.81	1.2173
8CB + 0.2 wt% GO	1.03	2.68	86.95	13.05	1.24	1.3294
8CB + 0.3 wt% GO	0.95	1.40	59.73	40.27	1.12	1.0605
8CB + 0.4 wt% GO	0.20	1.10	4.3	95.7	1.06	1.0722

Table 2: Fluorescence decay parameters of 8CB and 8CB+GO mixtures fitted by bi-exponential fit.

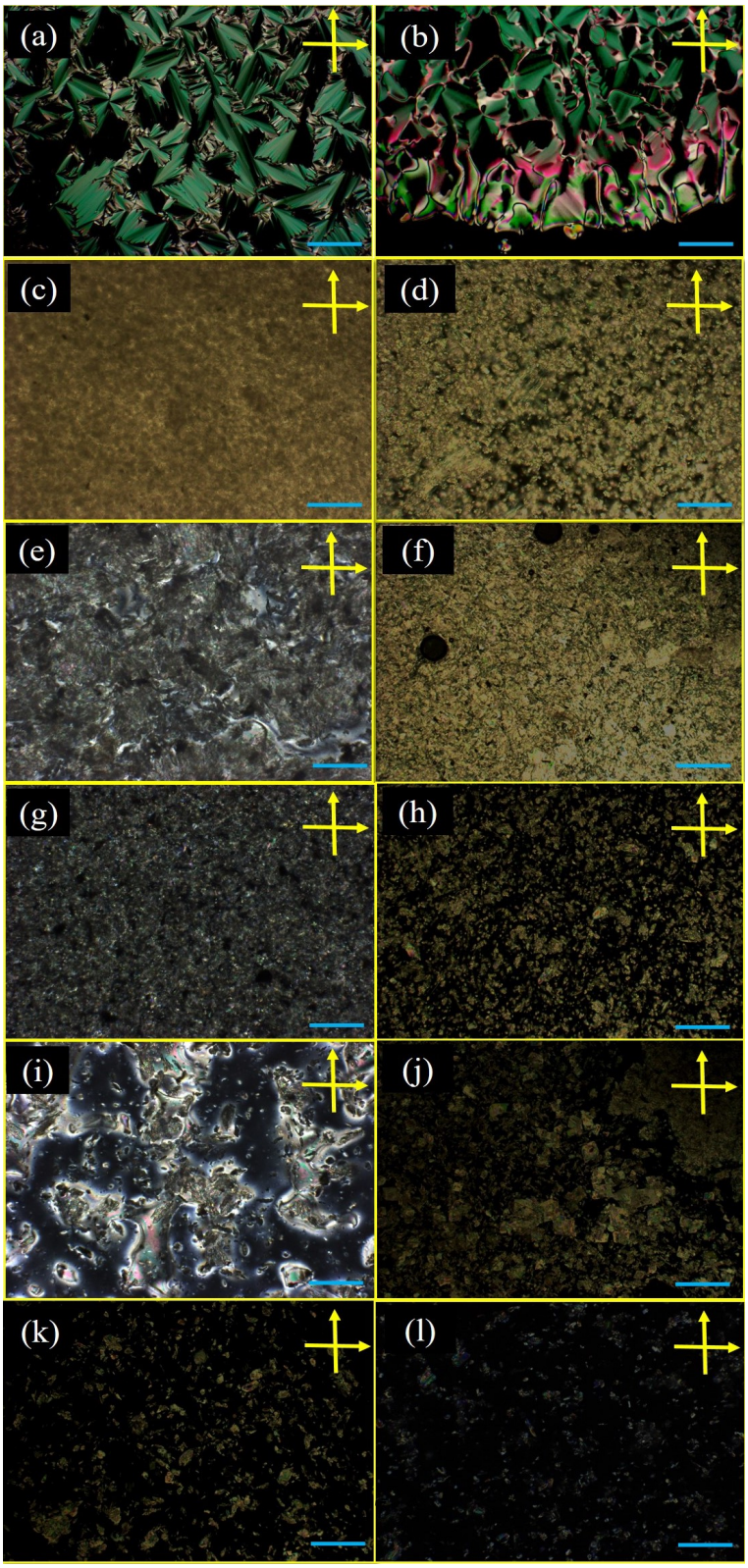

Figure 3: Polarized optical micrographs (POMs) of the (a),(b) 8CB, (c),(d) 8CB + 0.02, (e),(f) 8CB + 0.1, (g),(h) 8CB + 0.2, (i),(j) 8CB + 0.3 and (k),(l) 8CB + 0.4 wt% dispersion of 2D-GO nanoflakes in the smectic A and nematic phases, respectively. The crossed arrows represent the crossed polarizer-analyzer condition at which POMs have been taken. The scale bar is 100 μm in all POMs.

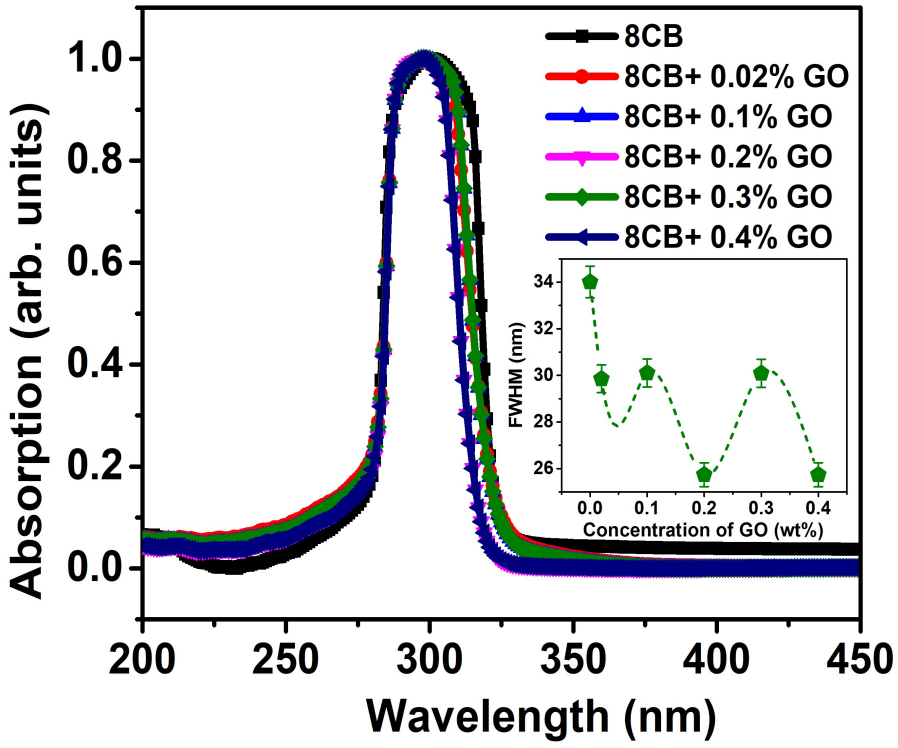

Figure 4: Absorption spectra of the 8CB and its composites with 2D-GO nanoflakes. Inset shows the variation of full width at half maxima (FWHM) of absorption band with the variation of dispersion concentration of GO. The concentration of solution was equivalent to 1mg/ml.

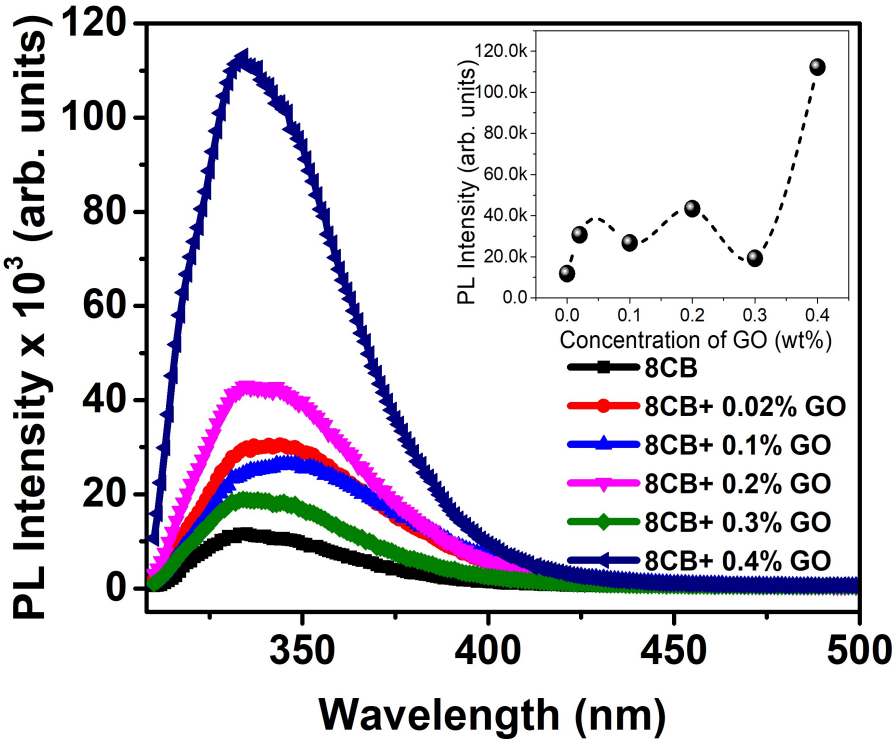

Figure 5: Photoluminescence (PL) spectra of the 8CB and its composites having different 2D-GO nanoflakes as a function of wavelength. Inset represents the variation of PL intensity with the change in the dispersion concentration of GO. The concentration of solution was equivalent to 1mg/ml.

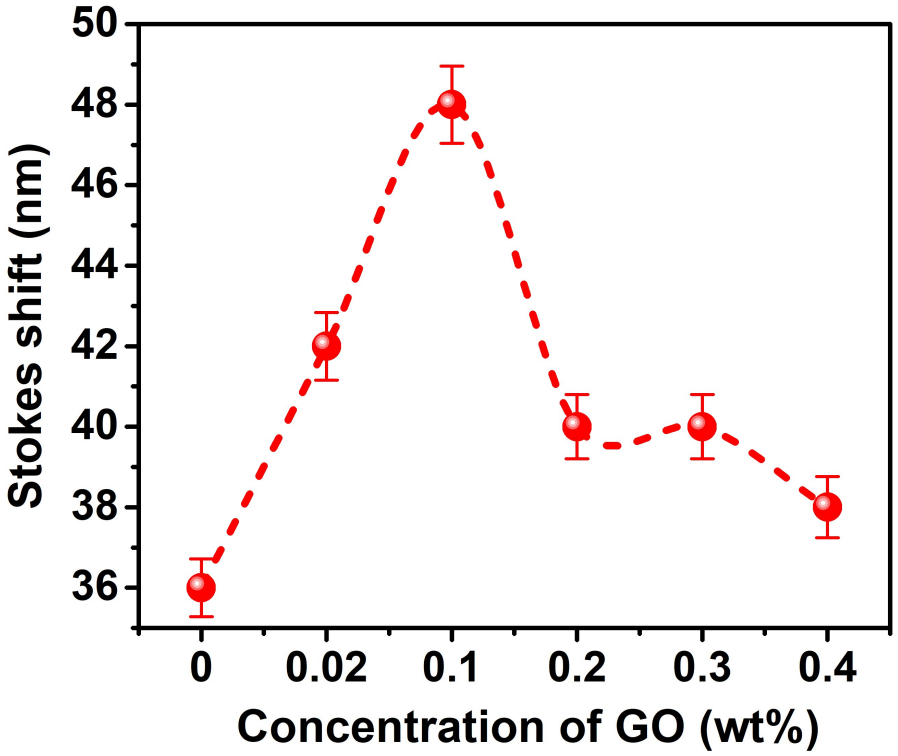

Figure 6: Stokes shift of the pure 8CB LC and it's composites having different concentrations of 2D-GO nanoflakes.

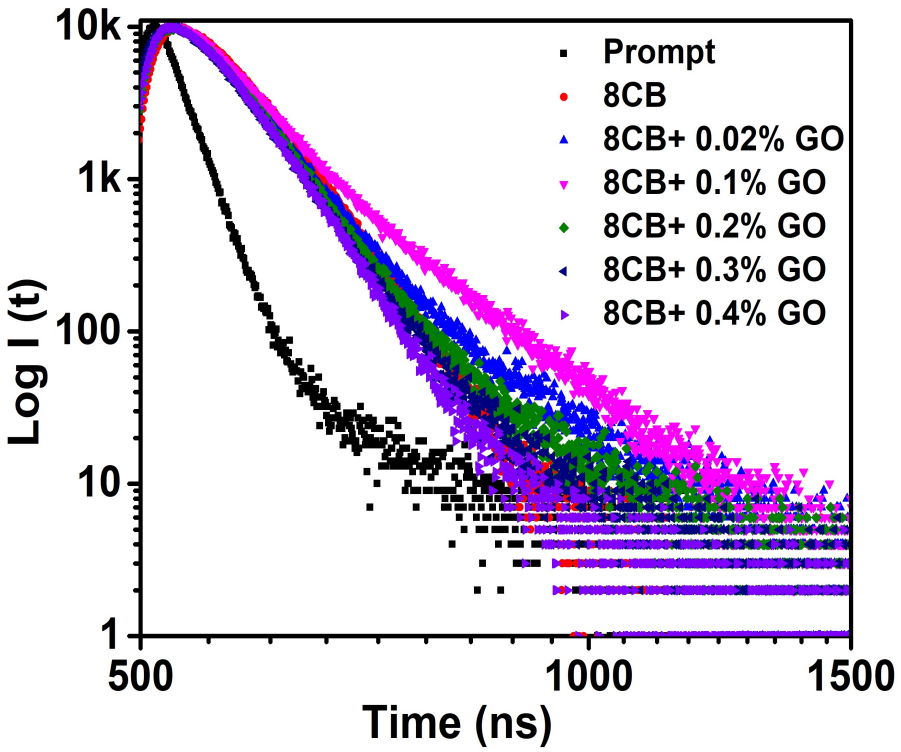

Figure 7: Time-resolved decay profile of the 8CB LC and it's composites having different concentrations of 2D-GO nanoflakes. The 8CB-GO pairs were excited by 296 nm wavelength.

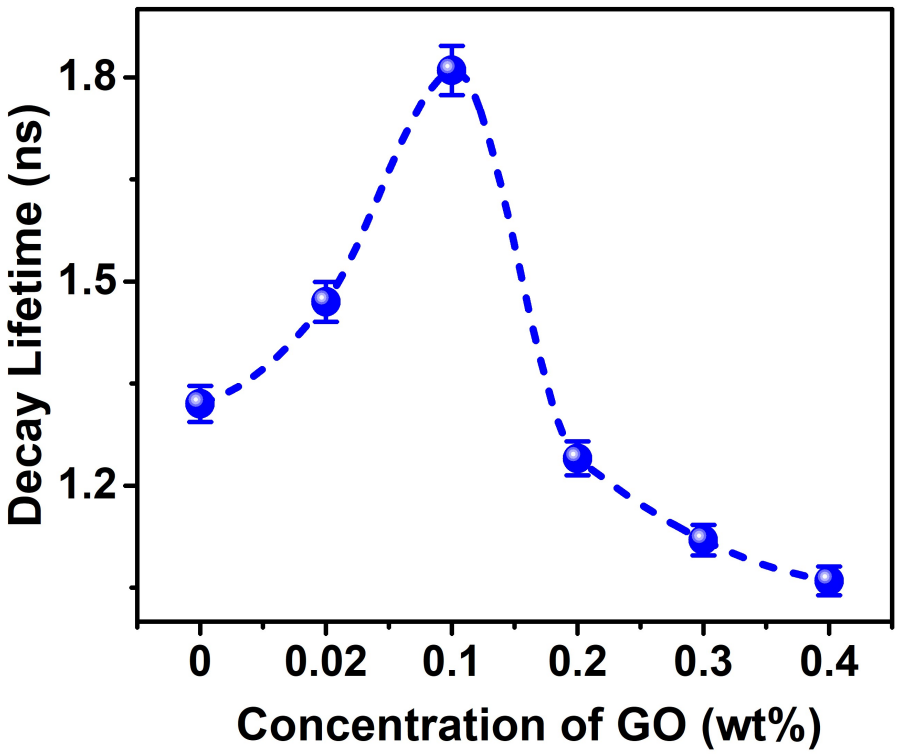

Figure 8: Variation of average decay lifetime with the change in 2D-GO nanoflakes concentrations in the 8CB LC.

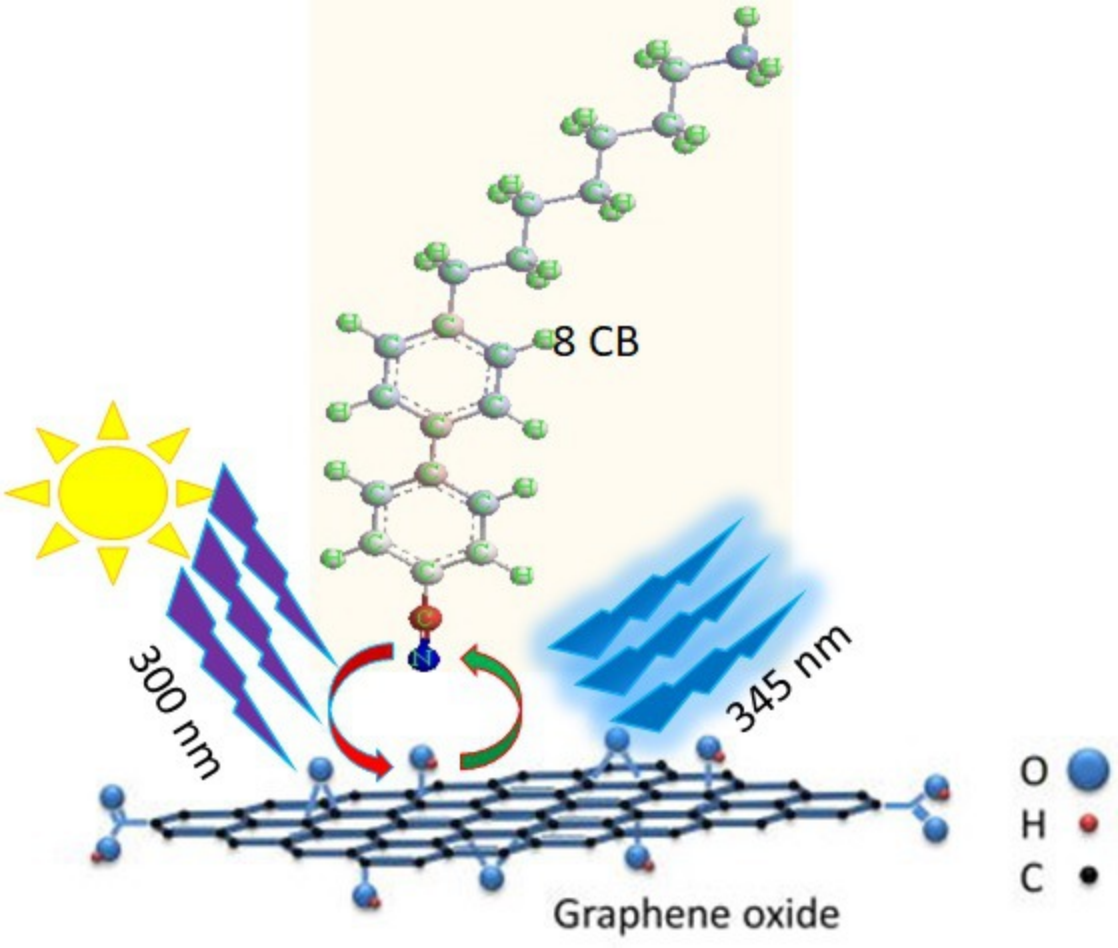
8 CB
300 nm
345 nm
O
H
C
Graphene oxide